Article

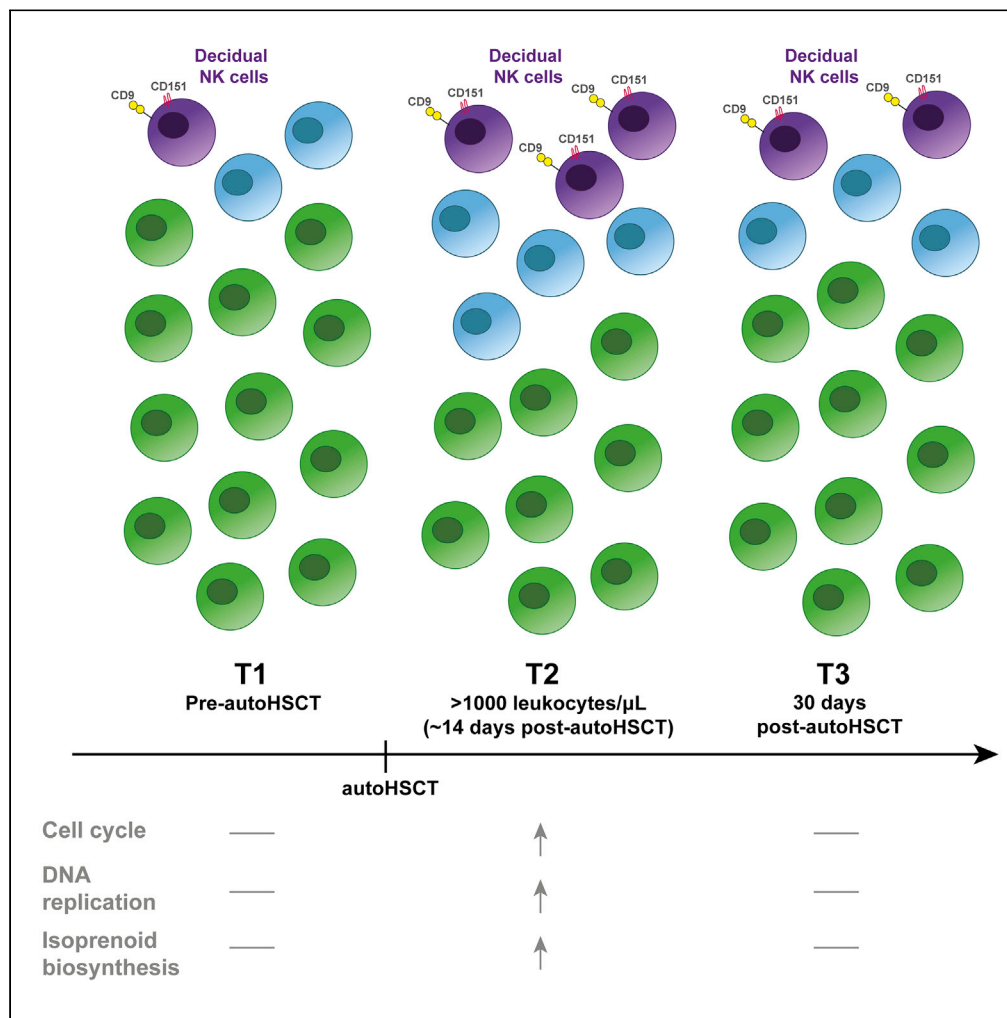# *In vivo* expansion of a CD9⁺ decidual-like NK cell subset following autologous hematopoietic stem cell transplantation

Ane Orrantia, Enrique Vázquez-De Luis, Gabirel Astarloa-Pando, ..., Ana Dopazo, Olatz Zenarruzabeitia, Francisco Borrego

francisco.borregorabasco@osakidetza.eus

Highlights

The transcriptome of NK cells is significantly altered immediately after autoHSCT

The synthesis of isoprenoids is upregulated during NK cell pool reconstitution

There is an expansion of CD9⁺ decidual-like NK cells following autoHSCT

Article

In vivo expansion of a CD9+ decidual-like NK cell subset following autologous hematopoietic stem cell transplantation

Ane Orrantia,[1,8] Enrique Vázquez-De Luis,[2,8] Gabirel Astarloa-Pando,[1] Iñigo Terrén,[1] Ainhoa Amarilla-Irusta,[1] Diego Polanco-Alonso,[1] Carmen González,[3] Alasne Uranga,[3] Tomás Carrascosa,[4] Juan J. Mateos-Mazón,[5] Juan C. García-Ruiz,[5] Sergio Callejas,[2] Ana Quintas,[2] Ana Dopazo,[2,6] Olatz Zenarruzabeitia,[1] and Francisco Borrego[1,7,9,*]

SUMMARY

Autologous hematopoietic stem cell transplantation (autoHSCT) is a treatment option for hematological disorders and pediatric solid tumors. After an autoHSCT, natural killer (NK) cells are the first lymphocyte subset returning to normal levels. To uncover global changes during NK cell reconstitution after autoHSCT, we performed RNA-sequencing on NK cells before and after autoHSCT. Results showed profound changes in the gene expression profile of NK cells immediately after autoHSCT. Several biological processes including cell cycle, DNA replication and the mevalonate pathway were enriched. Significantly, we observed that following autoHSCT, NK cells acquired a decidual-like gene expression profile, including the expression of CD9. By using multiparametric flow cytometry, we confirmed the expansion of NK cells expressing CD9 immediately after autoHSCT, which exhibited higher granzyme B and perforin expression levels than CD9⁻ NK cells. These results provide insights into the physiopathology of NK cells during their reconstitution after autoHSCT.

INTRODUCTION

Autologous hematopoietic stem cell transplantation (autoHSCT) is a therapy indicated to treat a diverse group of hematological malignances and pediatric solid tumors (Bazinet and Popradi, 2019; Copelan, 2006; Hale, 2005). An early immune recovery after autoHSCT and specifically, day 15 absolute lymphocyte count (ALC-15) after autoHSCT, have been described as an independent prognostic indicator for different types of cancers (Porrata et al., 2001a, 2001b, 2002a, 2002b). Among lymphocytes, natural killer (NK) cells are the first to recover during immune reconstitution after transplantation (Porrata et al., 2001c; Storek et al., 2008) and are recognized as the main lymphocyte subset in ALC-15 that affects outcome after autoHSCT (Porrata et al., 2008).

NK cells are innate lymphocytes with the capacity to recognize and eliminate virus-infected and malignant cells without prior sensitization (Cooper et al., 2001). Although traditionally divided in two main subsets (CD56^bright and CD56^dim), NK cells are a diverse population of cells that exhibit different phenotypic and functional features depending on tissue localization, maturation stage, environmental stimuli, viral infections, cancer, etc. (Freud et al., 2017). For example, tissue-resident NK cells express very high levels of CD56 and markers of residency such as CD103, CD69, and CD49a (Crinier et al., 2018; Freud et al., 2017). Decidual NK (dNK) cells are an interesting tissue-resident NK cell subset that exhibit a distinct phenotype and unique transcriptional profile in comparison to peripheral blood NK (pNK) cells (Koopman et al., 2003). dNK cells have been described as poorly cytotoxic, although they express functional activating receptors and complete lytic machinery (Jabrane-Ferrat, 2019). Moreover, they are able to produce several cytokines, such as interferon-gamma (IFNγ), tumor necrosis factor (TNF), granulocyte-macrophage colony-stimulating factor (GM-CSF), transforming growth factor β (TGF-β), and interleukin (IL)-10; chemokines, including, IL-8, macrophage inflammatory protein 1 alpha (MIP1α), MIP1β, CCL5, CXCL10 and CXCL12; and angiogenic factors including angiopoietin-2, placental growth factor (PLGF) and vascular endothelial growth factor (VEGF), at least after stimulation with IL-2 or IL-15 (Jabrane-Ferrat, 2019). dNK cells have been shown to regulate key

[1]Immunopathology Group, Biocruces Bizkaia Health Research Institute, 48903 Barakaldo, Spain

[2]Genomics Unit, Spanish National Center for Cardiovascular Research (CNIC), 28029 Madrid, Spain

[3]Biodonostia Health Research Institute, Hematology and Hemotherapy Service, Donostia University Hospital, 20014 Donostia-San Sebastián, Spain

[4]Hematological Cancer Group, Biocruces Bizkaia Health Research Institute, Hematology and Hemotherapy Service, Galdakao-Usansolo University Hospital, 48960 Galdakao, Spain

[5]Hematological Cancer Group, Biocruces Bizkaia Health Research Institute, Hematology and Hemotherapy Service, Cruces University Hospital, 48903 Barakaldo, Spain

[6]CIBER de Enfermedades Cardiovasculares (CIBERCV), Madrid, Spain

[7]Ikerbasque, Basque Foundation for Science, 48013 Bilbao, Spain

[8]These authors contributed equally

[9]Lead contact

*Correspondence: francisco.borregorabasco@osakidetza.eus

https://doi.org/10.1016/j.isci.2022.105235

developmental processes during pregnancy, such as trophoblast invasion and vascular remodeling in the decidua (Hanna et al., 2006). On the other hand, it is well known that both tumor-associated and tumor-infiltrating NK cells (TANK and TINK, respectively) exhibit altered phenotype, metabolic profile, and effector functions (Bruno et al., 2013; Terrén et al., 2019, 2020; Terrén and Borrego, 2022).

The phenotype diversity has also been observed when NK cell subsets reconstitution after autoHSCT was analyzed in patients with multiple myeloma (MM) and malignant lymphomas (Jacobs et al., 2015; Orrantia et al., 2021). Specifically, immediately after autoHSCT, NK cells exhibited an immature phenotype and higher proliferation capacity (Orrantia et al., 2021) and showed differential expression of killer immuno-globulin-like receptors (KIRs) (Jacobs et al., 2015) compared to NK cells pre-transplant. However, these phenotypic changes were not maintained overtime (Jacobs et al., 2015; Orrantia et al., 2021). Importantly, we have previously described an association between NK cells' maturation stage after autoHSCT and the clinical outcome of patients with MM (Orrantia et al., 2021). Thus, with the aim of acquiring a broader knowledge of NK cell biology and physiopathology, we performed RNA-sequencing (RNA-seq) of NK cells during their reconstitution after autoHSCT. Our results demonstrate that the gene expression profile of NK cells exhibits very significant changes and that an intriguing decidual-like NK cell subset is expanded following autoHSCT.

RESULTS

The transcriptome landscape of natural killer cells is significantly changed during the hematopoietic reconstitution after autologous hematopoietic stem cell transplantation

NK cells undergo profound phenotypical changes following autoHSCT (Jacobs et al., 2015; Orrantia et al., 2021). To gain further insight into other aspects of NK cell biology, as for example proliferation and metabolism, during subset reconstitution after autoHSCT, the gene expression profile of NK cells from patients with MM (cohort 1) undergoing autoHSCT were compared at three different time points: T1 (pre-transplantation), T2 (after leukocyte recovery or >1000 leukocytes/μL, usually around day 14 after autoHSCT) and T3 (30 days after autoHSCT). The clinical characteristics of patients from cohort 1 are listed in Table 1.

Differential gene expression analysis revealed changes in the gene expression profile of NK cells during their reconstitution, mainly at T2. Specifically, 194 genes were upregulated and 220 were downregulated in T2 compared to T1, and 197 genes were upregulated and 257 were downregulated in T2 compared to T3 (Figure 1A). In contrast, only few genes were altered in T3 compared to T1 (Figure 1B). Moreover, un-supervised hierarchical cluster analysis demonstrated a shift in gene expression pattern at T2 (Figure 1C). In general, genes were clearly separated into two main groups with different gene expression profiles. The first group (G1) consisted of genes with high expression in T2 compared to T1 and T3, and in contrast, the fourth group (G4) consisted of genes with low expression in T2 that were highly expressed at T1 and T3. However, as revealed by genes in groups G2 and G3 that showed lower expression in T3 than in T1 and higher expression in T3 than in T1, respectively, NK cell gene profile was similar but not identical at T3 compared to T1 (Figure 1C). This suggests that some changes persist in NK cells gene profile one month (T3) after autoHSCT.

Cell division is a highly relevant biological process in natural killer cells early after autologous hematopoietic stem cell transplantation

Over representation analysis (ORA) performed against the Reactome database (Gillespie et al., 2022) revealed that the 10 most significantly enriched pathways for upregulated genes at T2, compared to both T1 and T3, were pathways associated with cell cycle and DNA replication (Figure 1D). Similar results were obtained with Gene Ontology database (Carbon et al., 2021) (Figure S1). However, cell cycle and DNA replication pathways were not enriched when ORA was performed with upregulated genes in T3 compared to T1, indicating that while early after autoHSCT NK cells are vigorously dividing, one month after autoHSCT (T3) NK cells recover pre-transplant (T1) division rate, confirming our previous results (Orrantia et al., 2021).

The synthesis of isoprenoids is significantly upregulated during natural killer cell pool reconstitution

Although cell division and DNA replication were the most significantly enriched pathways at T2 compared to T1, gene set enrichment analysis (GSEA) against the Kyoto Encyclopedia of Genes and

Table 1. Cohort 1: Multiple myeloma patients' clinical characteristics

		n (%)
Gender	Male	10 (52.6%)
	Female	9 (47.4%)
Myeloma classification: ISS	ISS1	4 (21.1%)
	ISS2	9 (47.4%)
	ISS3	5 (26.3%)
Myeloma classification: Durie-Salmon Staging System	I-A	2 (10.5%)
	II-A	4 (21.1%)
	III-A	9 (47.4%)
	III-B	1 (5.3%)
Mobilization regimen	G-CSF	18 (94.7%)
	Plerixafor	1 (5.3%)
Conditioning regimen	Melphalan 200	17 (89.5%)
	Melphalan 140 + BUMEL	2 (10.5%)
CMV serostatus	Yes	18 (94.7%)
	No	1 (5.3%)
Maintenance or consolidation regimen	Yes	14 (73.7%)
	No	5 (26.3%)
Tandem autoHSCT	Yes	9 (47.4%)
	No	10 (52.6%)
Disease progression	Yes	11 (57.9%)
	No	8 (42.1%)
		Median (interquartile range)
Age		59 (46–72)
Infused CD34$^+$ cells (x10^6 cells/kg)		2.73 (2.01–5.59)

ISS indicates International Staging System; G-CSF: granulocyte colony-stimulating factor BUMEL, busulfan-melphalan; CMV, cytomegalovirus.

Genomes (KEGG) database (Kanehisa et al., 2021) also revealed an upregulation of metabolic pathways (normalized enrichment score or NES: 2.76; adjusted p value: $3x10^{-10}$). Among differentially expressed genes (DEGs) we found that *GAPDH* and *ENO1*, which encode two key enzymes of glycolysis, were upregulated at T2 compared to T1; *SUCLA2* and *FH*, which encode enzymes that are part of the tricarboxylic acid cycle and *ACAA2*, which encode an enzyme involved in fatty acid β-oxidation, were also upregulated at T2 (Figure 2A). Specifically, ORA of upregulated genes against the KEGG modules database showed an overrepresentation of the mevalonate pathway and pathways associated with nucleotide metabolism (Figure 2B). The mevalonate pathway, which is part of the terpenoid backbone biosynthetic pathway, is responsible for the synthesis of isopentenyl pyrophosphate, the essential building block of all isoprenoids including cholesterol. As shown in Figure 2C, genes encoding most of the key enzymes of the mevalonate pathway appeared upregulated at T2 compared to T1: *ACAT1, ACAT2, HMGCS1, HMGCR, PMVK,* and *MVD*. These results suggest that the synthesis of isoprenoids is key for NK cells early after autoHSCT.

Natural killer cells acquire a decidual-like gene expression profile early after autologous hematopoietic stem cell transplantation

Once the functional enrichment analysis was completed, we focused on the analysis of individual DEGs to further characterize alterations in gene expression profiles that occur during NK cell reconstitution following autoHSCT. We observed that a number of genes related to NK cell development and maturation (*LEF1, ZEB2, FCRL6*), cytotoxicity (*LGALS1, LGALS3, GZMB, TNFSF10, FCGR3A*), genes encoding activating receptors and activation markers (*CD300C, CD38, CD160*) and chemokine receptors (*CCR1, CCR5, CCR7*) were differentially expressed at T2 compared to T1 (Figure 2A). Surprisingly, among the
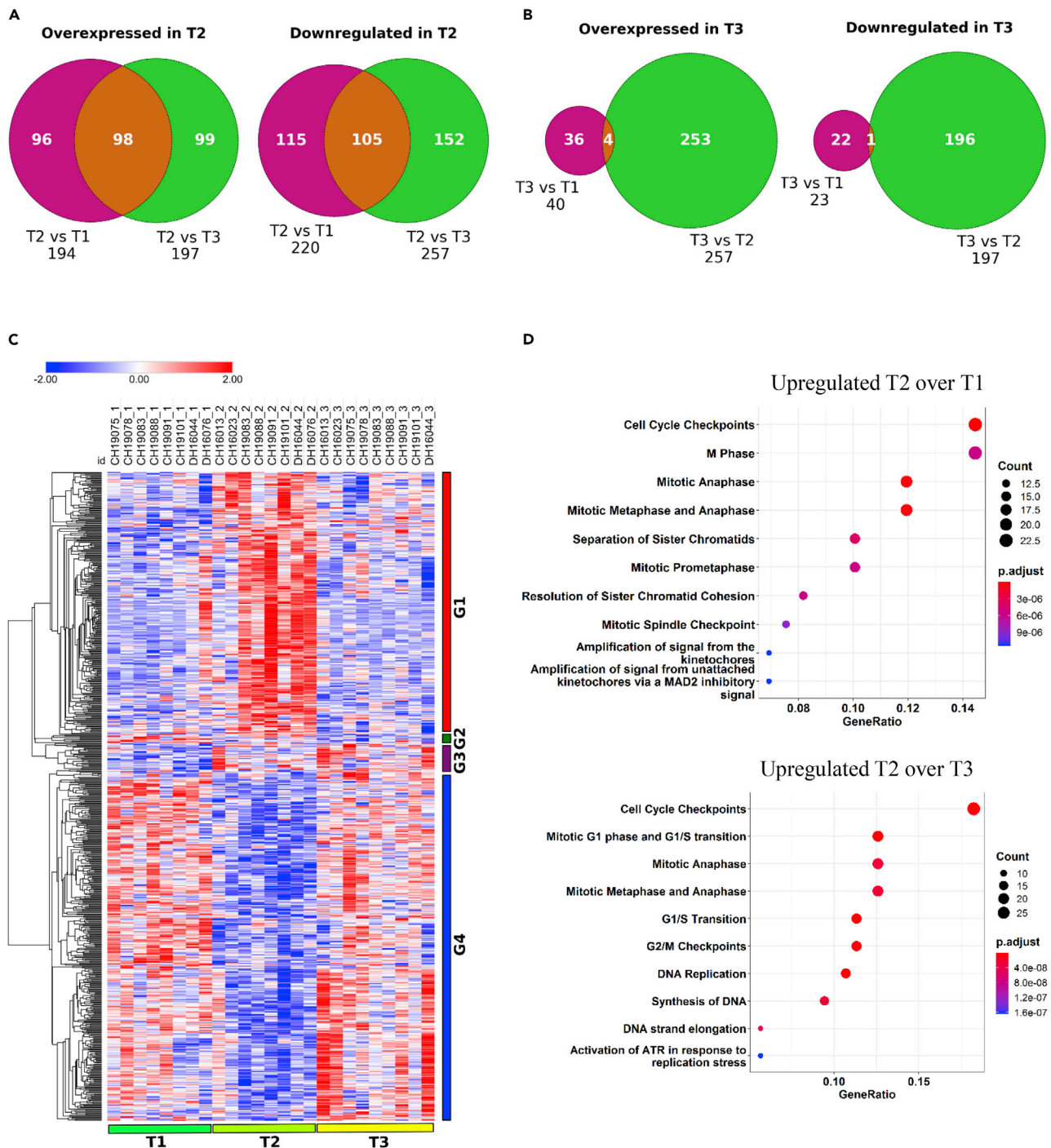
Figure 1. The gene expression profile of NK cells significantly changes immediately after autoHSCT

(A) Venn diagrams showing the number of differentially expressed genes (DEGs) in T2 compared to T1 and T3.

(B) Venn diagrams showing the number of DEGs in T3 compared to T1 and T2.

(C) Heatmap showing the relative expression of DEGs in the three-time points (T1, T2, and T3). Genes were hierarchically grouped according to their homology. Patients' samples (in columns) were grouped based on the time points (T1, T2, and T3). Four gene groups were identified according to the gene expression pattern profile among time points (G1, G2, G3, and G4). G1 consists of genes with high expression in T2 compared to T1 and T3; G2 consists of

Figure 1. *Continued*

genes with lower expression in T3 than in T1; G3 consists of genes with higher expression in T3 than in T1; and G4 consists of genes with lower expression in T2 compared to T1 and T3.

(D) Enrichment dot plot graphs showing the 10 most significant upregulated biological processes at T2 compared to T1 (upper panel) and T3 (lower panel). Reactome database was used for this analysis. Samples from 10 patients with MM, from cohort 1, were used for RNA-seq analysis.

top 10 DEGs with lower p value and higher Log_2FC value in T2 vs T1 comparison, we found *CD9*, which encodes a protein from the tetraspanin family. Although CD9 is ubiquitously expressed by all the major subsets of leukocytes, it is considered a marker to be mostly expressed on decidual NK (dNK) cells (Koopman et al., 2003). The upregulation of *CD9* at T2 was confirmed by qPCR (Figure S2).

In contrast to peripheral blood NK (pNK) cell subsets (CD56^{bright} and CD56^{dim} NK cells), dNK cells have been described to, among others, express CD9, CD151, tetraspan-5 (*TSPAN5*), Glycodelin A (*PAEP*) and Core 2β-1,6-N-acetylglucosaminyl transferase (*GCNT1*) (Koopman et al., 2003). In addition, as other tissue-resident NK cells, dNK cells also show expression of CD103 (*ITGAE*) and CD49a (*ITGA1*) (Jabrane-Ferrat, 2019). As shown in Figure 3A, NK cells showed a significantly higher expression of *CD9* and *CD151* at T2 compared to both T1 and T3. Moreover, although not statistically significant, the mean expression of *TSPAN5*, *GCNT1*, and *PAEP* tended to be slightly higher at T2. Furthermore, they showed higher expression of galectin-1 (*LGALS1*), which has been described to be overexpressed in dNK cells in comparison to pNK cells (Koopman et al., 2003). Like CD56^{dim} NK cells, dNK are known to express KIRs although the repertoire seems to be different compared with pNK cells (Koopman et al., 2003). The analysis of the detected KIRs revealed an interesting increment in the expression of *KIR2DL4* at T2 compared to T1 (Figure 3A). The ligand for this KIR is the non-classical HLA-G molecule whose expression is restricted to the fetal trophoblast cells that invade the maternal decidua during early pregnancy (Rajagopalan and Long, 2012). Similar results were obtained for *ITGA1* (CD49a) and *ITGAE* (CD103) (Figure 3A). The chemokine receptors CXCR3 and CXCR4 seem to mediate the traffic of dNK toward maternal-fetal interface (Albini and Noonan, 2021). Results also demonstrated a tendency to an upregulation of *CXCR3* at T2 and a tendency to an upregulation of *CXCR4* at T3 (Figure 3A). Together, these data suggest that NK cells acquire a decidual-like (dNK-like) gene expression profile early after autoHSCT (T2) that is not maintained overtime.

A subset of CD9^{+} natural killer cells is expanded early after autologous hematopoietic stem cell transplantation

Given the functional differences between pNK cells and dNK cells (Jabrane-Ferrat, 2019), we were interested in studying the effector functions of CD9^{+} NK cells expanded after autoHSCT and comparing them with the CD9^{−} NK cell subset. For that, we first examined degranulation (CD107a), cytokine (IFNγ, TNF, and IL-10), and chemokine production (IL-8, MIP1β) after stimulation with PMA and ionomycin in patients with MM (cohort 1). Of note, this unspecific stimulation is not a substitute for a cytotoxic assay, but it allowed to measure NK cell effector functions regardless of the possible differences that CD9^{+} and CD9^{−} NK cells may show in the expression of activating and inhibitory receptors. In addition, we have determined effector functions (CD107a, IFNγ, TNF, and MIP1β) after stimulating NK cells with the 721.221 target cell line in a heterogeneous cohort of patients (cohort 2) who also underwent autoHSCT (Table 2). Furthermore, we evaluated the content of lytic granules of non-stimulated NK cells by measuring granzyme B and perforin expression levels.

First, we observed that patients before the autoHSCT (T1) exhibited a higher frequency of CD9^{+} NK cells than healthy donors (Figure 3B), which is consistent with previous data showing that CD9^{+} NK cells are expanded in patients with cancer (Albini and Noonan, 2021; Bruno et al., 2018; Gallazzi et al., 2021; Kim et al., 2016). Second, flow cytometry data are in agreement with the results obtained with RNA-seq and clearly showed an expansion of CD9^{+} NK cells early after autoHSCT (T2) (Figure 3C). The frequency of CD9^{+} NK cells at T2 was higher than the frequency before the autoHSCT (T1) and 30 days after (T3) the autoHSCT (Figure 3C). Interestingly, at T3 it was observed that the frequency of CD9^{+} NK cells was still higher than before the autoHSCT (T1) (Figure 3C), which is somehow consistent with the qPCR data (Figure S2).

Next, we analyzed granzyme B and perforin expression and found that CD9^{+} NK cells exhibited higher expression of these two important components of lytic granules compared to CD9^{−} NK cells, as determined by the median fluorescence intensity (MFI) of these markers (Figure 3D). Although the differences were not statistically significant when we analyzed samples from cohort 2, probably owing to low number of samples, CD9^{+} NK cells have a clear tendency to express higher levels of perforin and granzyme B (Figure 3D).
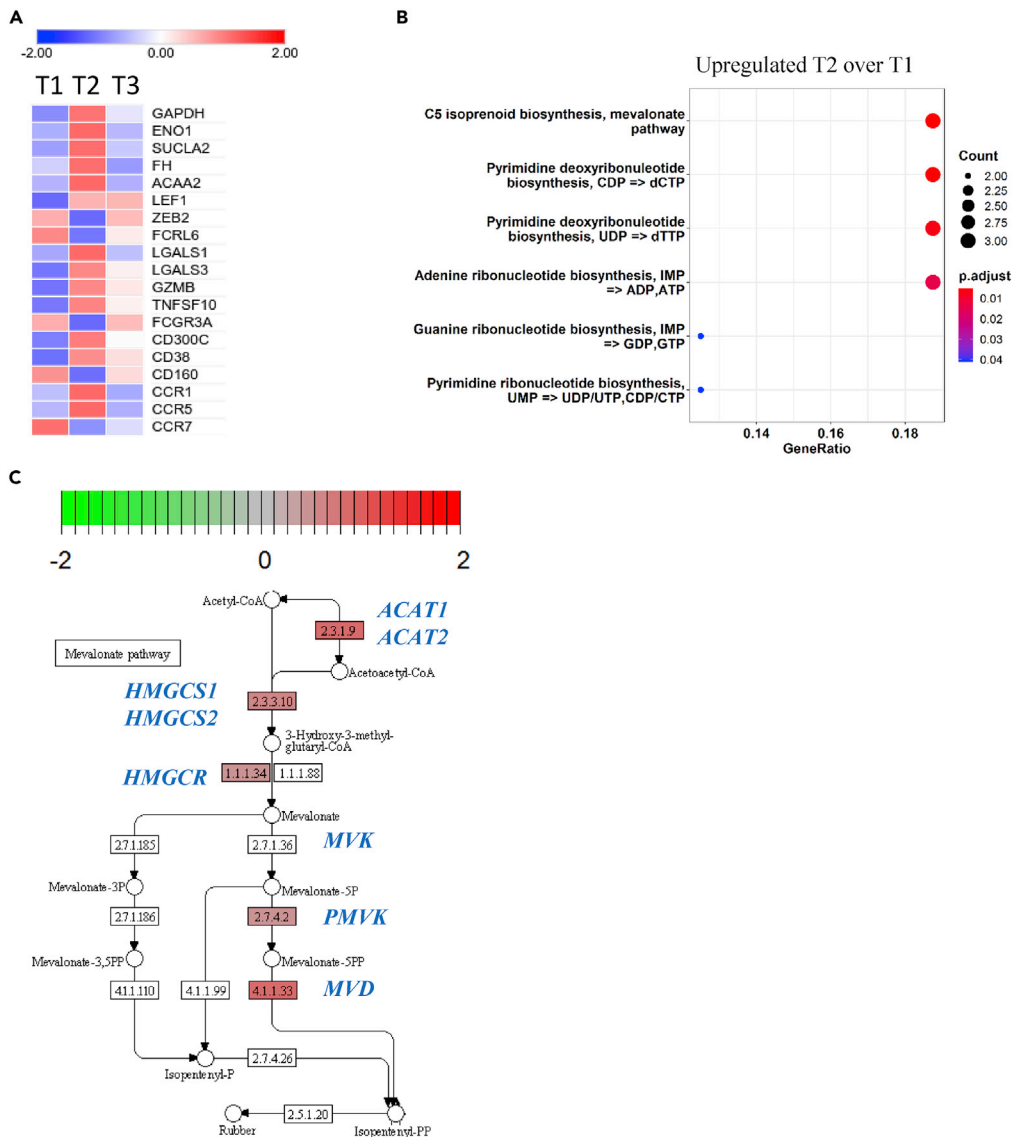
Figure 2. Metabolic pathways are upregulated at T2

(A) Heatmap showing the mean relative expression of genes related to metabolism (*GAPDH, ENO1, SUCLA2, FH, ACAA2*), to NK cell development and maturation (*LEF1, ZEB2, FCRL6*), cytotoxicity (*LGALS1, LGALS3, GZMB, TNFSF10, FCGR3A*) and genes encoding activating receptors and activation markers (*CD300C, CD38, CD160*) and chemokine receptors (*CCR1, CCR5, CCR7*) at the three-time points (T1, T2 and T3). (B) Enrichment dot plot graphs showing upregulated biological processes at T2 over T1. KEGG modules database was used for this analysis. Modules are ranked based on the gene ratio. The size of the dot represents the number of genes upregulated within each category and the color of the dot represents the significance of the enrichment.

(C) A portion of the KEGG pathway map of the terpenoid backbone biosynthesis (hsa00900), showing the mevalonate pathway at T2 over T1. The color inside the boxes refers to the Log$_2$FC. The number inside the boxes refers to KEGG identification numbers, which represent the gene or gene family found at that position in the pathway. Samples from 10 patients with MM, from cohort 1, were used for RNA-seq analysis.

Regarding effector functions in response to PMA and ionomycin, our results showed lower frequency of CD107a+ cells, indicating a lower degranulation, in addition to a tendency to a lower frequency of MIP1β+ cells within CD9$^+$ NK cells compared to CD9$^-$ NK cells (Figure S3A). No significant IL-8 expression was observed in NK cells (data not shown). Furthermore, no clear differences in cytokine production (IFNγ, TNF, IL-10) were observed between CD9$^+$ and CD9$^-$ NK cells (Figure S3A), except
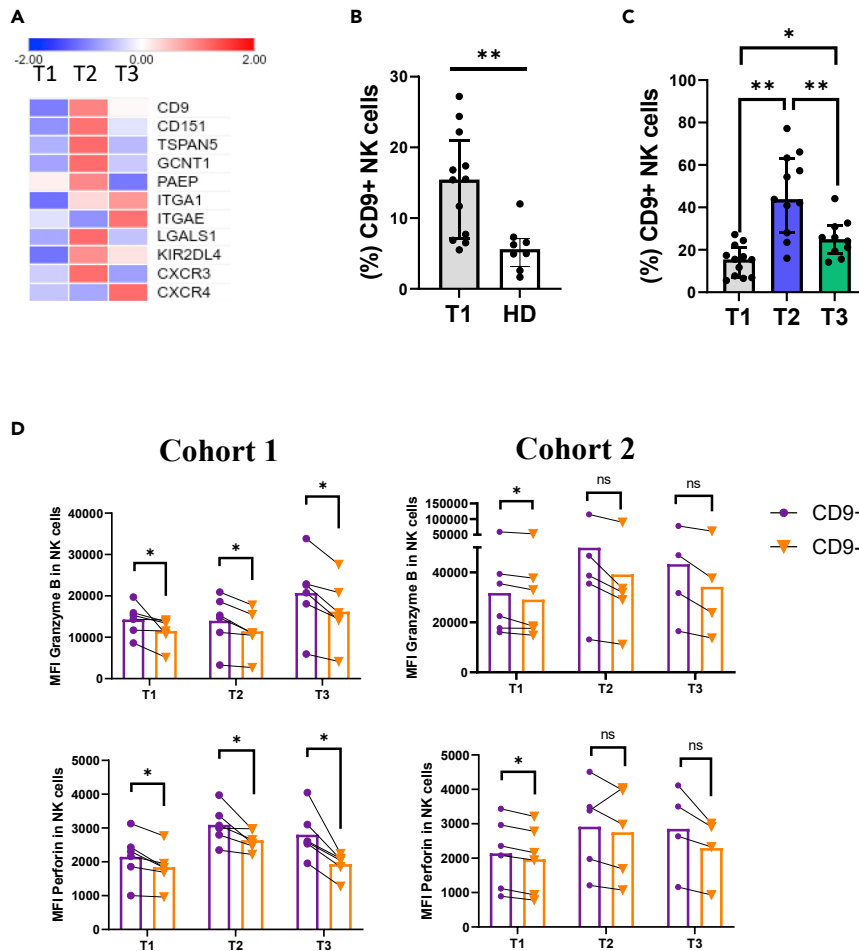
Figure 3. NK cells acquire a dNK-like phenotype immediately after autoHSCT

(A) Heatmap showing the mean relative expression of genes related to dNK cell phenotype at the three-time points (T1, T2, and T3). Samples from 10 patients with MM, from cohort 1, were used for RNA-seq analysis.

(B) Bar graph showing the frequency of CD9+ NK cells from 12 patients (6 from cohort 1 and 6 from cohort 2) and 8 healthy donors (HD). Each dot represents a donor. Significance of the data was determined by using Mann-Whitney test comparing ranks for unpaired and non-parametric data. Data were represented as bar plots showing the median and interquartile range. **$p < 0.01$.

(C) Bar graph showing the frequency of CD9+ NK cells at T1, T2, T3 from 12 patients (6 patients from cohort 1 and 6 patients from cohort 2) undergoing autoHSCT. Significance of the data was determined by using Wilcoxon matched pairs signed rank test. Each dot represents a patient. Data were represented as bar plots showing the median and interquartile range. *$p < 0.05$, **$p < 0.01$.

(D) Bar graphs showing the MFI of granzyme B (upper line) and perforin (lower line) within CD9+ or CD9− NK cells at T1, T2, T3. Each dot represents a patient. Samples from 6 patients from cohort 1 (left) and 6 patients from cohort 2 (right) were used in this analysis. Significance of the data was determined by using Wilcoxon matched pairs signed rank test. Bars represent the mean. ns: not significant, *$p < 0.05$.

for IFNγ at T3 and TNF at T2. Although we do not have an explanation for these data, it may be possible that, although statistically significant, the biological relevance may be minimal. On the other hand, there were no significant differences between CD9+ and CD9− NK cells regarding degranulation (CD107a) and cytokine production (MIP1β, TNF, and IFNγ) following the stimulation with the 721.221 target cell line (Figure S3B). Together, these results suggest that CD9+ NK cells that expanded early after autoHSCT have higher levels of granzyme B and perforin and may exhibit some altered effector functions (CD107a and MIP1β) that depend on the type of stimulus (PMA and ionomycin versus 721.221 target cell line).

Table 2. Cohort 2: Patients' clinical characteristics

		n (%)
Gender	Male	4 (66.7%)
	Female	2 (33.3%)
Cancer type	POEMS syndrome	2 (33.3%)
	Amyloidosis	2 (33.3%)
	Multiple myeloma	1 (16.7%)
	AML	1 (16.7%)
Mobilization regimen	G-CSF	4 (66.7%)
	Plerixafor	1 (16.7%)
	G-CSF + Plerixafor	1 (16.7%)
		Median (interquartile range)
Age		58.50 (49.00–66.25)
Infused CD34$^+$ cells (x10^6 cells/kg)		2.51 (2.19–2.82)

POEMS stands for polyneuropathy, organomegaly, endocrinopathy, M protein, and skin changes. G-CSF: granulocyte colony-stimulating factor; AML: Acute myeloid leukemia.

DISCUSSION

In this study, we have examined the global changes occurring in NK cells during their reconstitution after human HSCT, by analyzing their transcriptome using RNA-seq technology. We have documented that the gene expression profile of NK cells changes immediately after leukocyte recovery, being the cell cycle the main biological process at this point. Moreover, we have also described the upregulation of some metabolic pathways, such as the mevalonate pathway. We have also found that NK cells acquire a dNK-like phenotype shortly after autoHSCT and that these cells show some differences when compared with conventional NK cells.

Flow cytometry-based studies have previously reported that NK cells undergo a phenotypic change after autoHSCT (Jacobs et al., 2015; Orrantia et al., 2021). In line with these data, our RNA-seq results have demonstrated that the gene expression profile of NK cells changes early after autoHSCT (T2). Moreover, although the transcriptome landscapes of NK cells at pre-transplant (T1) and 30 days after (T3) autoHSCT are similar, they show certain differences, which is also in accordance with previous studies (Orrantia et al., 2021). Among the overexpressed genes on T3 vs T1 some examples include *CD9*, *CD55*, *KIR2DL3*, *KIR3DL1*, *KIR2DL4*, *KIR2DS4*, and *GZMB*. Among the downregulated genes on T3 vs T1 some examples include *CCR7*, *PECAM1*, *FCRL6* and *TGFBR1*.

An early immune recovery after both alloHSCT and autoHSCT is key for patients' outcome (Pavletic et al., 1998; Porrata et al., 2001a, 2001b, 2002a, 2002b). Early lymphocyte recovery, and more importantly, early NK cell recovery were reported to predict superior survival after autoHSCT (Porrata et al., 2008; Rueff et al., 2014). Moreover, NK cells have been described as the first lymphocyte population to be recovered to normal levels after autoHSCT, being NK cell count and functionality restored as early as day 14 post-transplant (Porrata et al., 2001c; Storek et al., 2008). Therefore, it is not unexpected that the major changes in the gene expression profile of NK cells occur before T3 (30 days after autoHSCT). Our data demonstrate that, immediately after transplantation, NK cells are in the active phase of the cell cycle and that DNA replication and nucleotide metabolism are upregulated. However, the upregulation of these biological processes is not maintained 30 days after autoHSCT. These findings are in agreement with the dramatic increase in the frequency of Ki67-expressing cells immediately after autoHSCT (Orrantia et al., 2021), suggesting that one of the biological processes that NK cells are undergoing is cell division to reach pre-transplant counts, process that appear to be completed one-month post-autoHSCT (T3).

NK cells have been described to exhibit an immature phenotype at leukocyte recovery and NK cell maturation occurs during their reconstitution after autoHSCT (Orrantia et al., 2021). Similar to what occurs with T cells (Bantug et al., 2018), studies conducted in the last years indicate that NK cell differentiation status is closely associated with their metabolic signature (Marçais et al., 2014; Terrén et al., 2020). Moreover, NK cell

metabolism can also be modified by other processes, such as cell activation and some pathological conditions (O'Brien and Finlay, 2019; Terrén et al., 2019, 2020). In this regard, our data demonstrate an upregulation of metabolic pathways, specifically of the mevalonate pathway, immediately after autoHSCT. Mevalonate is the precursor of isoprenoids, such as cholesterol that is a key component of the eukaryotic cell membranes. This pathway is known to be essential for lymphocyte proliferation and cell cycle progression (Chakrabarti and Engleman, 1991; Crosbie et al., 2013; Cuthbert and Lipsky, 1990) which, in turn, is consistent with the above-presented data. In addition, the mevalonate pathway is also important for NK cell cytotoxicity (Crosbie et al., 2013; Poggi et al., 2013). Fluvastatin, an inhibitor of the 3-hydroxy-3-methylglutaryl-coenzyme A (HMG-CoA) encoded by the *HMGCR* gene, is known to inhibit actin redistribution, RhoA activation (needed for acting assembly), and lipid raft formation (Poggi et al., 2013). In addition, fluvastatin inhibits the intracellular free calcium increase, Akt1/PKB activation mediated by activating receptors engagement, and perforin/granzyme-containing granules release (Poggi et al., 2013). All these effects were reverted with the addition of mevalonate (Poggi et al., 2013). Thus, the synthesis of mevalonate is essential for the cytoskeleton assembly and influence NK cell activation and cytotoxic granules release (Poggi et al., 2013).

Our data revealed, to our knowledge, a previously undescribed shift in NK cells phenotype toward a dNK-like phenotype immediately after autoHSCT. pNK can acquire characteristics of dNK cells, such as the expression of CD9, by their culture with not only conditioned medium from decidual stromal cells, but also with TGF-β1 (Keskin et al., 2007). Conversion of pNK into a dNK-like phenotype is also achieved under hypoxia and TGF-β1 culture conditions (Cerdeira et al., 2013). In addition, induction of the expression of CD9 is also observed when NK cells are activated with IL-2 and PHA (Hanna et al., 2004). Very recently, it has been reported that, in co-culture experiments, the NK-92 cell line acquires CD9 from ovarian tumor cell lines through trogocytosis (Gonzalez et al., 2021). However, the acquisition of dNK-like phenotype after autoHSCT may not be explained by these mechanisms. In fact, the TGF-β1 serum levels were reported to be reduced during autologous bone marrow transplantation conditioning regimen and returned to normal levels between days 20 and 50 post-transplant (Coomes and Moore, 2010; Liem et al., 1999). Nevertheless, the combination of TGF-β1 with IL-15 and/or IL-18, cytokines also produced by decidual stroma cells, similarly induced the acquisition of dNK cell markers (Du et al., 2022; Hawke et al., 2020; Siewiera et al., 2015). Very significantly, IL-15 plasma levels are highly increased after autoHSCT (Orrantia et al., 2021; Porrata et al., 2010) that, together with TGF-β1, may in part contribute to the acquisition of the dNK-like phenotype. Thus, we hypothesize that the unique cytokine milieu that is present immediately after autoHSCT may be responsible for this change in the NK cell phenotype.

Besides a distinct phenotype, dNK cells also show different functional characteristics compared to pNK cells. dNK cells play crucial roles during pregnancy, such as regulating trophoblast invasion and promoting vascular growth in the decidua (Hanna et al., 2006). These functions are mediated by the secretion of different cytokines and chemokines. For example, dNK cells secrete IL-8 and interferon-inducible protein 10, which, upon binding to their receptors expressed on the trophoblast, regulate its invasion. Moreover, dNK cells secrete angiogenic growth factors, such as VEGF and PLGF, which promote vascular remodeling (Jabrane-Ferrat, 2019; Zhang et al., 2021). Although they display abundant cytolytic granules (Koopman et al., 2003), dNK cells present low cytotoxic effect toward the K562 cell line (King et al., 1996) and failed to polarize their microtubules organizing centers and cytotoxic granules to the immunological synapse (Kopcow et al., 2005). However, very recently it was demonstrated that dNK cells protect placenta from infections via selective transfer of granulysin (Crespo et al., 2020; Liu et al., 2021). In addition to dNK cells, TINK and tumor-associated NK cells from patients with non-small-cell lung carcinoma (NSCLC) were also found to secrete proangiogenic factors, such as VEGF, PLGF, and IL-8 (Bruno et al., 2013, 2014). In this case, the proangiogenic activity of NK cells in tumors could have detrimental actions (Albini and Noonan, 2021). Finally, the acquisition of CD9 from high-grade serous ovarian tumor cells via trogocytosis was shown to confer NK cells immunosuppressive properties (Gonzalez et al., 2021).

Although CD9$^+$ NK cells express higher levels of perforin and granzyme B than CD9$^-$ NK cells, it is unclear to what extent the effector functions of these subsets are different, especially regarding degranulation (CD107a) and MIP1β production. Several possibilities may explain the different results we have obtained with different stimuli and cohorts (Figure S3): 1) PMA and ionomycin stimulation is a very strong and non-specific stimulus, whereas the stimulation of 721.221 target cells is specific and, it may occur, that other types of stimuli (i.e., other target cells, proinflammatory cytokines, etc.) give rise to different results. 2) The two cohorts of patients with different types of cancer may affect NK cell activity differently.

3) Overnight priming with IL-15 (see STAR Methods section) could obliterate differences between CD9$^+$ and CD9$^-$cells in response to 721.221 target cells. Regardless, what is clear is that more research is needed to fully define this highly expanded NK cell subset after autoHSCT.

The expansion of the CD9$^+$ NK cell subset early after autoHSCT may have clinical implications. Several publications have signaled that the increased frequency of CD9$^+$ circulating immune cells associates with worse disease-free survival in patients with cancer (Albini and Noonan, 2021; Bruno et al., 2018; Gallazzi et al., 2021; Kim et al., 2016). Also, an important issue is the impact of the infused autograft absolute lymphocyte count. In addition to stem cells, infusion of autograft immune effector cells produces an autologous graft-versus-tumor effect (Porrata, 2022). We have not determined the number of CD9$^+$ NK cells infused from the autograft and, undoubtedly, this is a point that needs to be investigated in future studies to determine the role of this NK cell subset in the evolution of patients undergoing autoHSCT.

In conclusion, to our knowledge, this is the first study to perform RNA-seq in NK cells from patients undergoing HSCT. We have demonstrated a change in the gene expression profile of NK cells shortly after autoHSCT, with an upregulation of biological processes such as cell cycle and metabolism. We have also revealed that NK cells acquire a phenotype similar to that of dNK cells, characterized by the expression of CD9. These CD9$^+$ NK cells express higher levels of perforin and granzyme B and, depending on the stimuli, they may exhibit different effector functions when compared with CD9$^-$ NK cells. Future studies will determine the relevance of decidual-like NK cells in HSCT. Despite the limitation in the number of samples analyzed, the results presented here provide insights into the biology and physiopathology of NK cells during their reconstitution after autoHSCT.

Limitations of the study

In this study, we have shown that the NK cell transcriptome changes significantly immediately after autoHSCT (around days 14-15). Thirty days after transplantation, NK cell gene expression is very similar to, but not the same as, that of pre-transplant NK cells. We have analyzed the bulk NK cell transcriptome using RNA-seq, which assesses changes owing to experimental conditions (before and after transplantation). However, these analyzes did not allow us to assess differences between NK cell subsets. For that, single-cell RNA-seq analyses (scRNA-seq) must be performed. Also, extensive flow cytometry, mass cytometry, or spectral cytometry studies can be helpful in phenotypically defining CD9$^+$ decidual NK cells. In addition, we have only preliminarily defined the functional profile of CD9$^+$ NK cells, so it is essential to fully characterize their effector functions, including testing their proangiogenic activity, in response to different stimuli. Finally, if the expansion of CD9$^+$ decidual-type NK cells, or other characteristics, are associated with disease prognosis after autoHSCT, it is necessary to carry out this type of study in a larger cohort of patients.

STAR★METHODS

Detailed methods are provided in the online version of this paper and include the following:

- KEY RESOURCES TABLE
- RESOURCE AVAILABILITY
  - Lead contact
  - Materials availability
  - Data and code availability
- EXPERIMENTAL MODEL AND SUBJECT DETAILS
  - Patients' characteristics and study design
- METHOD DETAILS
  - Sample preparation
  - NK cell isolation
  - RNA extraction and sequencing
  - Reverse transcription (RT) reaction
  - Real time qPCR
  - Flow cytometry: Functional assay
- QUANTIFICATION AND STATISTICAL ANALYSIS
  - RNA-seq data analysis
  - Flow cytometry data analysis

AUTHOR CONTRIBUTIONS

F.B. and O.Z. conceived the project; F.B., A.O., E.V-DL., S.C., A.Q., and A.D. designed experiments; C.G., A.U., T.C., J.J.M-M. and J.C.G-R. obtained the clinical samples and clinical data from patients; A.O., G.A-P and D.P-A. performed experiments; A.O. and E.V-DL. performed data analysis; A.O. and E.V-DL. designed figures; F.B., I.T., G.A-P., A.A-I., and O.Z. provided intellectual input; F.B. and A.O. wrote the article; all authors critically reviewed the article.

DECLARATION OF INTERESTS

The authors declare no competing interests.

REFERENCES

Albini, A., and Noonan, D.M. (2021). Decidual-like NK cell polarization: from cancer killing to cancer nurturing. Cancer Discov. 11, 28–33. https://doi.org/10.1158/2159-8290.CD-20-0796.

Bantug, G.R., Galluzzi, L., Kroemer, G., and Hess, C. (2018). The spectrum of T cell metabolism in health and disease. Nat. Rev. Immunol. 18, 19–34. https://doi.org/10.1038/nri.2017.99.

Bazinet, A., and Popradi, G. (2019). A general practitioner's guide to hematopoietic stem-cell transplantation. Curr. Oncol. 26, 187–191. https://doi.org/10.3747/co.26.5033.

Bruno, A., Bassani, B., D'Urso, D.G., Pitaku, I., Cassinotti, E., Pelosi, G., Boni, L., Dominioni, L., Noonan, D.M., Mortara, L., and Albini, A. (2018). Angiogenin and the MMP9-TIMP2 axis are up-regulated in proangiogenic, decidual NK-like cells from patients with colorectal cancer. FASEB J. 32, 5365–5377. https://doi.org/10.1096/fj.201701103R.

Bruno, A., Ferlazzo, G., Albini, A., and Noonan, D.M. (2014). A think tank of TINK/TANKs: tumor-infiltrating/tumor-associated natural killer cells in tumor progression and angiogenesis. J. Natl. Cancer Inst. 106. dju200–13. https://doi.org/10.1093/jnci/dju200.

Bruno, A., Focaccetti, C., Pagani, A., Imperatori, A.S., Spagnoletti, M., Rotolo, N., Cantelmo, A.R., Franzi, F., Capella, C., Ferlazzo, G., et al. (2013). The proangiogenic phenotype of natural killer cells in patients with non-small cell lung cancer. Neoplasia 15, 133–142. https://doi.org/10.1593/neo.121758.

Carbon, S., Douglass, E., Good, B.M., Unni, D.R., Harris, N.L., Mungall, C.J., Basu, S., Chisholm, R.L., Dodson, R.J., Hartline, E., et al. (2021). The Gene Ontology resource: enriching a GOld mine. Nucleic Acids Res. 49, D325–D334. https://doi.org/10.1093/nar/gkaa1113.

Cerdeira, A.S., Rajakumar, A., Royle, C.M., Lo, A., Husain, Z., Thadhani, R.I., Sukhatme, V.P., Karumanchi, S.A., and Kopcow, H.D. (2013). Conversion of peripheral blood NK cells to a decidual NK-like phenotype by a cocktail of defined factors. J. Immunol. 190, 3939–3948. https://doi.org/10.4049/jimmunol.1202582.

Chakrabarti, R., and Engleman, E.G. (1991). Interrelationships between mevalonate metabolism and the mitogenic signaling pathway in T lymphocyte proliferation. J. Biol. Chem. 266, 12216–12222. https://doi.org/10.1016/S0021-9258(18)98884-8.

Coomes, S.M., and Moore, B.B. (2010). Pleiotropic effects of transforming growth factor-β in hematopoietic stem-cell transplantation. Transplantation 90, 1139–1144. https://doi.org/10.1097/TP.0b013e3181efd018.

Cooper, M.A., Fehniger, T.A., and Caligiuri, M.A. (2001). The biology of human natural killer-cell subsets. Trends Immunol. 22, 633–640. https://doi.org/10.1016/s1471-4906(01)02060-9.

Copelan, E.A. (2006). Hematopoietic stem-cell transplantation. N. Engl. J. Med. 354, 1813–1826. https://doi.org/10.1056/NEJMra052638.

Crespo, Â.C., Mulik, S., Dotiwala, F., Ansara, J.A., Sen Santara, S., Ingersoll, K., Ovies, C., Junqueira, C., Tilburgs, T., Strominger, J.L., and Lieberman, J. (2020). Decidual NK cells transfer granulysin to selectively kill bacteria in trophoblasts. Cell 182, 1125–1139.e18. https://doi.org/10.1016/j.cell.2020.07.019.

Crinier, A., Milpied, P., Escalière, B., Piperoglou, C., Galluso, J., Balsamo, A., Spinelli, L., Cervera-

Marzal, I., Ebbo, M., Girard-Madoux, M., et al. (2018). High-dimensional single-cell analysis identifies organ-specific signatures and conserved NK cell subsets in humans and mice. Immunity 49, 971–986.e5. https://doi.org/10.1016/j.immuni.2018.09.009.

Crosbie, J., Magnussen, M., Dornbier, R., Iannone, A., and Steele, T.A. (2013). Statins inhibit proliferation and cytotoxicity of a human leukemic natural killer cell line. Biomark. Res. 1, 33. https://doi.org/10.1186/2050-7771-1-33.

Cuthbert, J.A., and Lipsky, P.E. (1990). Inhibition by 6-fluoromevalonate demonstrates that mevalonate or one of the mevalonate phosphates is necessary for lymphocyte proliferation. J. Biol. Chem. 265, 18568–18575. https://doi.org/10.1016/S0021-9258(17)44789-2.

Du, X., Zhu, H., Jiao, D., Nian, Z., Zhang, J., Zhou, Y., Zheng, X., Tong, X., Wei, H., and Fu, B. (2022). Human-induced CD49a+ NK cells promote fetal growth. Front. Immunol. 13, 821542–821613. https://doi.org/10.3389/fimmu.2022.821542.

Freud, A.G., Mundy-Bosse, B.L., Yu, J., and Caligiuri, M.A. (2017). The Broad spectrum of human natural killer cell diversity. Immunity. https://doi.org/10.1016/j.immuni.2017.10.008.

Gallazzi, M., Baci, D., Mortara, L., Bosi, A., Buono, G., Naselli, A., Guarneri, A., Dehò, F., Capogrosso, P., Albini, A., et al. (2021). Prostate cancer peripheral blood NK cells show enhanced CD9, CD49a, CXCR4, CXCL8, MMP-9 production and secrete monocyte-recruiting and polarizing factors. Front. Immunol. 11, 586126–586217. https://doi.org/10.3389/fimmu.2020.586126.

Gillespie, M., Jassal, B., Stephan, R., Milacic, M., Rothfels, K., Senff-Ribeiro, A., Griss, J., Sevilla, C., Matthews, L., Gong, C., et al. (2022). The reactome pathway knowledgebase 2022. Nucleic Acids Res. 50, D687–D692. https://doi.org/10.1093/nar/gkab1028.

Gonzalez, V.D., Huang, Y.-W., Delgado-Gonzalez, A., Chen, S.-Y., Donoso, K., Sachs, K., Gentles, A.J., Allard, G.M., Kolahi, K.S., Howitt, B.E., et al. (2021). High-grade serous ovarian tumor cells modulate NK cell function to create an immune-tolerant microenvironment. Cell Rep. 36, 109632. https://doi.org/10.1016/j.celrep.2021.109632.

Hale, G.A. (2005). Autologous hematopoietic stem cell transplantation for pediatric solid tumors. Expert Rev. Anticancer Ther. 5, 835–846. https://doi.org/10.1586/14737140.5.5.835.

Hanna, J., Bechtel, P., Zhai, Y., Youssef, F., McLachlan, K., and Mandelboim, O. (2004). Novel insights on human NK cells' immunological modalities revealed by gene expression profiling. J. Immunol. 173, 6547–6563. https://doi.org/10.4049/jimmunol.173.11.6547.

Hanna, J., Goldman-Wohl, D., Hamani, Y., Avraham, I., Greenfield, C., Natanson-Yaron, S., Prus, D., Cohen-Daniel, L., Arnon, T.I., Manaster, I., et al. (2006). Decidual NK cells regulate key developmental processes at the human fetal-maternal interface. Nat. Med. 12, 1065–1074. https://doi.org/10.1038/nm1452.

Hawke, L.G., Mitchell, B.Z., and Ormiston, M.L. (2020). TGF-B and IL-15 synergize through MAPK pathways to drive the conversion of human NK cells to an innate lymphoid cell 1–like phenotype. J. Immunol. 204, 3171–3181. https://doi.org/10.4049/jimmunol.1900866.

Jabrane-Ferrat, N. (2019). Features of human decidual NK cells in healthy pregnancy and during viral infection. Front. Immunol. 10, 1397–1410. https://doi.org/10.3389/fimmu.2019.01397.

Jacobs, B., Tognarelli, S., Poller, K., Bader, P., Mackensen, A., and Ullrich, E. (2015). NK cell subgroups, phenotype, and functions after autologous stem cell transplantation. Front. Immunol. 6, 583. https://doi.org/10.3389/fimmu.2015.00583.

Kanehisa, M., Furumichi, M., Sato, Y., Ishiguro-Watanabe, M., and Tanabe, M. (2021). KEGG: integrating viruses and cellular organisms. Nucleic Acids Res. 49, D545–D551. https://doi.org/10.1093/nar/gkaa970.

Keskin, D.B., Allan, D.S.J., Rybalov, B., Andzelm, M.M., Stern, J.N.H., Kopcow, H.D., Koopman, L.A., and Strominger, J.L. (2007). TGFbeta promotes conversion of CD16+ peripheral blood NK cells into CD16- NK cells with similarities to decidual NK cells. Proc. Natl. Acad. Sci. USA 104, 3378–3383. https://doi.org/10.1073/pnas.0611098104.

Kim, K.-J., Kwon, H.J., Kim, M.C., and Bae, Y.K. (2016). CD9 expression in colorectal carcinomas and its prognostic significance. J. Pathol. Transl. Med. 50, 459–468. https://doi.org/10.4132/jptm.2016.10.02.

King, A., Jokhi, P.P., Burrows, T.D., Gardner, L., Sharkey, A.M., and Loke, Y.W. (1996). Functions of human decidual NK cells. Am. J. Reprod. Immunol. 35, 258–260. https://doi.org/10.1111/j.1600-0897.1996.tb00041.x.

Koopman, L.A., Kopcow, H.D., Rybalov, B., Boyson, J.E., Orange, J.S., Schatz, F., Masch, R., Lockwood, C.J., Schachter, A.D., Park, P.J., and Strominger, J.L. (2003). Human decidual natural killer cells are a unique NK cell subset with immunomodulatory Potential. J. Exp. Med. 198, 1201–1212. https://doi.org/10.1084/jem.20030305.

Kopcow, H.D., Allan, D.S.J., Chen, X., Rybalov, B., Andzelm, M.M., Ge, B., and Strominger, J.L. (2005). Human decidual NK cells form immature activating synapses and are not cytotoxic. Proc. Natl. Acad. Sci. USA 102, 15563–15568. https://doi.org/10.1073/pnas.0507835102.

Li, B., and Dewey, C.N. (2011). RSEM: accurate transcript quantification from RNA-Seq data with or without a reference genome. BMC Bioinf. 12, 323. https://doi.org/10.1186/1471-2105-12-323.

Liem, L.M., Fibbe, W.E., van Houwelingen, H.C., and Goulmy, E. (1999). Serum transforming growth factor-beta1 levels in bone marrow transplant recipients correlate with blood cell counts and chronic graft-versus-host disease. Transplantation 67, 59–65. https://doi.org/10.1097/00007890-199901150-00009.

Liu, Y., Gao, S., Zhao, Y., Wang, H., Pan, Q., and Shao, Q. (2021). Decidual natural killer cells: a good nanny at the maternal-fetal interface during early pregnancy. Front. Immunol. 12, 663660–663711. https://doi.org/10.3389/fimmu.2021.663660.

Luo, W., and Brouwer, C. (2013). Pathview: an R/Bioconductor package for pathway-based data integration and visualization. Bioinformatics 29, 1830–1831. https://doi.org/10.1093/bioinformatics/btt285.

Marçais, A., Cherfils-Vicini, J., Viant, C., Degouve, S., Viel, S., Fenis, A., Rabilloud, J., Mayol, K., Tavares, A., Bienvenu, J., et al. (2014). The metabolic checkpoint kinase mTOR is essential for IL-15 signaling during the development and activation of NK cells. Nat. Immunol. 15, 749–757. https://doi.org/10.1038/ni.2936.

O'Brien, K.L., and Finlay, D.K. (2019). Immunometabolism and natural killer cell responses. Nat. Rev. Immunol. 19, 282–290. https://doi.org/10.1038/s41577-019-0139-2.

Orrantia, A., Terrén, I., Astarloa-Pando, G., González, C., Uranga, A., Mateos-Mazón, J.J., García-Ruiz, J.C., Riñón, M., Rey, M., Pérez-Fernandez, S., et al. (2021). NK cell reconstitution after autologous hematopoietic stem cell transplantation: association between NK cell maturation stage and outcome in multiple myeloma. Front. Immunol. 12, 748207–748213. https://doi.org/10.3389/fimmu.2021.748207.

Orrantia, A., Terrén, I., Izquierdo-Lafuente, A., Alonso-Cabrera, J.A., Sandá, V., Vitallé, J., Moreno, S., Tasias, M., Uranga, A., González, C., et al. (2020). A NKp80-based identification strategy reveals that CD56neg NK cells are not completely dysfunctional in health and disease. iScience 23, 101298. https://doi.org/10.1016/j.isci.2020.101298.

Pavletic, Z.S., Joshi, S.S., Pirruccello, S.J., Tarantolo, S.R., Kollath, J., Reed, E.C., Bierman, P.J., Vose, J.M., Warkentin, P.I., Gross, T.G., et al. (1998). Lymphocyte reconstitution after allogeneic blood stem cell transplantation for hematologic malignancies. Bone Marrow Transplant. 21, 33–41. https://doi.org/10.1038/sj.bmt.1701037.

Poggi, A., Boero, S., Musso, A., and Zocchi, M.R. (2013). Selective role of mevalonate pathway in regulating perforin but not FasL and TNFalpha release in human natural killer cells. PLoS One 8, e62932. https://doi.org/10.1371/journal.pone.0062932.

Porrata, L.F., Ingle, J.N., Litzow, M.R., Geyer, S., and Markovic, S.N. (2001a). Prolonged survival associated with early lymphocyte recovery after autologous hematopoietic stem cell transplantation for patients with metastatic breast cancer. Bone Marrow Transplant. 28, 865–871. https://doi.org/10.1038/sj.bmt.1703236.

Porrata, L.F., Litzow, M.R., Tefferi, A., Letendre, L., Kumar, S., Geyer, S.M., and Markovic, S.N. (2002a). Early lymphocyte recovery is a predictive factor for prolonged survival after autologous hematopoietic stem cell transplantation for acute myelogenous leukemia. Leukemia 16, 1311–1318. https://doi.org/10.1038/sj.leu.2402503.

Porrata, L.F. (2022). The impact of infused autograft absolute numbers of immune effector cells on survival post-autologous stem cell transplantation. Cells 11, 2197. https://doi.org/10.3390/cells11142197.

Porrata, L.F., Gertz, M.A., Inwards, D.J., Litzow, M.R., Lacy, M.Q., Tefferi, A., Gastineau, D.A.,

Dispenzieri, A., Ansell, S.M., Micallef, I.N., et al. (2001b). Early lymphocyte recovery predicts superior survival after autologous hematopoietic stem cell transplantation in multiple myeloma or non-Hodgkin lymphoma. Blood *98*, 579–585. https://doi.org/10.1182/blood.V98.3.579.

Porrata, L.F., Inwards, D.J., Ansell, S.M., Micallef, I.N., Johnston, P.B., Gastineau, D.A., Litzow, M.R., Winters, J.L., and Markovic, S.N. (2008). Early lymphocyte recovery predicts superior survival after autologous stem cell transplantation in non-hodgkin lymphoma: a Prospective study. Biol. Blood Marrow Transplant. *14*, 807–816. https://doi.org/10.1016/j.bbmt.2008.04.013.

Porrata, L.F., Inwards, D.J., Micallef, I.N., Ansell, S.M., Geyer, S.M., and Markovic, S.N. (2002b). Early lymphocyte recovery post-autologous haematopoietic stem cell transplantation is associated with better survival in Hodgkin's disease. Br. J. Haematol. *117*, 629–633. https://doi.org/10.1046/j.1365-2141.2002.03478.x.

Porrata, L.F., Inwards, D.J., Micallef, I.N., Johnston, P.B., Ansell, S.M., Hogan, W.J., and Markovic, S.N. (2010). Interleukin-15 affects patient survival through natural killer cell recovery after autologous hematopoietic stem cell transplantation for non-hodgkin lymphomas. Clin. Dev. Immunol. 914945–13. https://doi.org/10.1155/2010/914945.

Porrata, L.F., Litzow, M.R., and Markovic, S.N. (2001). Immune reconstitution after autologous hematopoietic stem cell transplantation. Mayo Clin. Proc. *76*, 407–412. https://doi.org/10.4065/76.4.407.

Rajagopalan, S., and Long, E.O. (2012). KIR2DL4 (CD158d): an activation receptor for HLA-G. Front. Immunol. *3*, 258–266. https://doi.org/10.3389/fimmu.2012.00258.

Rueff, J., Medinger, M., Heim, D., Passweg, J., and Stern, M. (2014). Lymphocyte subset recovery and outcome after autologous hematopoietic stem cell transplantation for plasma cell myeloma. Biol. Blood Marrow Transplant. *20*, 896–899. https://doi.org/10.1016/j.bbmt.2014.03.007.

Siewiera, J., Gouilly, J., Hocine, H.-R., Cartron, G., Levy, C., Al-Daccak, R., and Jabrane-Ferrat, N. (2015). Natural cytotoxicity receptor splice variants orchestrate the distinct functions of human natural killer cell subtypes. Nat. Commun. *6*, 10183. https://doi.org/10.1038/ncomms10183.

Storek, J., Geddes, M., Khan, F., Huard, B., Helg, C., Chalandon, Y., Passweg, J., and Roosnek, E. (2008). Reconstitution of the immune system after hematopoietic stem cell transplantation in humans. Semin. Immunopathol. *30*, 425–437. https://doi.org/10.1007/s00281-008-0132-5.

Terrén, I., and Borrego, F. (2022). Role of NK cells in tumor progression. In Experientia Supplementum, Magdalena Klink and Izabela Szulc-Kielbic, eds. (Springer), pp. 169–187. https://doi.org/10.1007/978-3-030-91311-3.

Terrén, I., Orrantia, A., Vitallé, J., Astarloa-Pando, G., Zenarruzabeitia, O., and Borrego, F. (2020). Modulating NK cell metabolism for cancer immunotherapy. Semin. Hematol. *57*, 213–224. https://doi.org/10.1053/j.seminhematol.2020.10.003.

Terrén, I., Orrantia, A., Vitallé, J., Zenarruzabeitia, O., and Borrego, F. (2019). NK cell metabolism and tumor microenvironment. Front. Immunol. *10*, 2278. https://doi.org/10.3389/fimmu.2019.02278.

Yu, G., and He, Q.-Y. (2016). ReactomePA: an R/Bioconductor package for reactome pathway analysis and visualization. Mol. Biosyst. *12*, 477–479. https://doi.org/10.1039/C5MB00663E.

Yu, G., Wang, L.-G., Han, Y., and He, Q.-Y. (2012). clusterProfiler: an R Package for comparing biological themes among gene clusters. Omi. A J. Integr. Biol. *16*, 284–287. https://doi.org/10.1089/omi.2011.0118.

Zhang, X., Li, Y., Huang, C., Liu, S., Chen, X., Yu, S., Diao, L., and Zeng, Y. (2021). The role of decidual natural killer cell-derived soluble factors in early pregnancy. Am. J. Reprod. Immunol. *86*, e13477. https://doi.org/10.1111/aji.13477.

STAR★METHODS

KEY RESOURCES TABLE

REAGENT or RESOURCE	SOURCE	IDENTIFIER
Antibodies		
PE Mouse monoclonal antibody Anti-CD3 (UCHT1)	BD Biosciences	Cat#555333 RRID: AB_395740
PE Mouse monoclonal antibody Anti-CD14 (MφP9)	BD Biosciences	Cat#562691 RRID: AB_2737725
PE Mouse monoclonal antibody Anti-CD19 (HIB19)	BD Biosciences	Cat# 555413 RRID: AB_395813
PE-Cy5 Mouse monoclonal antibody Anti-CD56 (B159)	BD Biosciences	Cat# 555517 RRID: AB_395907
PE-Vio770 Mouse monoclonal antibody Anti-NKp80 (4A4.D10)	Miltenyi Biotec	Cat#130-105-068 RRID: AB_2659831
BV510 Mouse monoclonal antibody Anti-CD14 (MΦP9)	BD Biosciences	Cat#563079 RRID: AB_2737993
BV510 Mouse monoclonal antibody Anti-CD19 (SJ25C1)	BD Biosciences	Cat#562947 RRID: AB_2737914
BV510 Mouse monoclonal antibody Anti-CD123 (9F5)	BD Biosciences	Cat#563072 RRID: AB_2728102
BV786 Mouse monoclonal antibody Anti-CD56 (NCAM 16.2)	BD Biosciences	Cat#564058 RRID: AB_2738569
PerCP/Cyanine5.5 Mouse monoclonal antibody Anti-CD3 (SK7)	BioLegend	Cat#344808 RRID: AB_10640736
PE/Dazzle 594 Mouse monoclonal antibody Anti-CD9 (HI9a)	BioLegend	Cat#312118 RRID: AB_2728258
BV421 Mouse monoclonal antibody Anti-IL-8 (G265-8)	BD Biosciences	Cat#563310 RRID: AB_2738131
BV421 Mouse monoclonal antibody Anti-CD56 (NCAM 16.2)	BD Biosciences	Cat#562752 RRID: AB_2732054
BV605 Mouse monoclonal antibody Anti-IFN-γ (B27)	BD Biosciences	Cat#562974 RRID: AB_2737926
BV650 Rat monoclonal antibody Anti-IL-10 (JES3-9D7)	BD Biosciences	Cat#564051 RRID: AB_2738565
FITC Mouse monoclonal antibody Anti-MIP-1β (D21-1351)	BD Biosciences	Cat#560565 RRID: AB_1645489
R718 Mouse monoclonal antibody Anti-Granzyme B (GB11)	BD Biosciences	Cat#566964 RRID: AB_2869975
BV711 Mouse monoclonal antibody Anti-Perforin (dG9)	BioLegend	Cat#308130 RRID:AB_2687190
APC Mouse monoclonal antibody Anti-TNF-α (MAb11)	BioLegend	Cat#502912 RRID:AB_315264
APC-Vio770 Recombinant antibody RE-Afinity Anti-CD107a (REA792)	Miltenyi Biotec	Cat#130-111-623 RRID:AB_2654486
Biological samples		
PBMCs from multiple myeloma patients	Basque Biobank for Research	N/A

Continued

REAGENT or RESOURCE	SOURCE	IDENTIFIER
Chemicals, peptides, and recombinant proteins		
LIVE/DEAD™ Fixable Green Dead Cell Stain Kit for 488nm excitation	Invitrogen	Cat#L34969
LIVE/DEAD™ Fixable Aqua Dead Cell Stain Kit for 405nm excitation	Invitrogen	Cat#L34957
LIVE/DEAD™ Fixable Near IR Dead Cell Stain Kit for 633 or 635nm excitation	Invitrogen	Cat#10119
Brilliant Stain Buffer	BD Biosciences	N/A
GolgiStop™ Protein Transport Inhibitor (monensin)	BD Biosciences	Cat#554724
GolgiPlug™ Protein Transport Inhibitor (brefeldin A)	BD Biosciences	Cat#555029
Fixation/Permeablization Kit	BD Biosciences	Cat# 554714
Ficoll Paque Plus	GE Healthcare	Cat#GE17-1440-03
Fetal Bovine Serum (FBS)	GE Healthcare Hyclone	Cat#SV30160.03
Dimethyl sulfoxide (DMSO)	Thermo Scientific Scientific	Cat#20688
RPMI 1640 medium containing GlutaMAX	Gibco	Cat#72400054
Penicillin-Streptomycin	Gibco	Cat#15140122
MEM Non-Essential Amino Acids Solution (100X)	Gibco	Cat# 11140035
Sodium Pyruvate (100 mM)	Gibco	Cat# 11360070
PBS (PBS)	Gibco	Cat#18912
BSA	Millipore	Cat#A3733
Phorbol 12-myristate 13-acetate (PMA)	Merck	Cat# 79346
Ionomycin calcium salt from Streptomyces conglobatus	Merck	Cat# I0634
Critical commercial assays		
RNeasy Plus Micro Kit	Qiagen	Cat# 74034
NEBNext Single Cell/Low Input RNA Library Prep Kit for Illumina	New England Biolabs	Cat# E6420L
Super-Script IV VILO Master Mix with ezDNase enzyme	Invitrogen	Cat#11766050
Brilliant III Ultra-Fast SYBR Green qPCR Master Mix	Agilent Technologies	Cat# 600882
Deposited data		
	GEO (Gene Expression Omnibus)	GSE199608
Oligonucleotides		
Primer: PPIA Forward: CACCGTGTTCTTCGACATTG	Invitrogen	N/A
Primer: PPIA Reverse: CTGTGAAAGCAGGAACCCTTA	Invitrogen	N/A
Primer: CD9 Forward: GGGGATATTCCCACAAGGAT	Invitrogen	N/A
Primer: CD9 Reverse: GCAGTTCAACGCATAGTGGA	Invitrogen	N/A
Software and algorithms		
FlowJo™ Version 10.4.1	FlowJo	N/A
GraphPad Prism v9	GraphPad	N/A
AriaMX Real Time Software v.A1.2	Agilent Technologies	N/A
Rsem v.1.3.1	N/A	N/A
Morpheus	Broad Institute	N/A
clusterProfiler R package v.3.18.1	N/A	N/A

Continued		
REAGENT or RESOURCE	SOURCE	IDENTIFIER
ReactomePA R package v.1.34.0	N/A	N/A
Pathview R package v1.30.1	N/A	N/A

RESOURCE AVAILABILITY

Lead contact

Further information and requests for resources and reagents should be directed to and will be fulfilled by the lead contact, Francisco Borrego (francisco.borregorabasco@osakidetza.eus).

Materials availability

This study did not generate new unique reagents.

Data and code availability

- RNA-seq data have been deposited at GEO (Gene Expression Omnibus) and are publicly available as of the date of publication. Accession numbers are listed in the key resources table.
- All custom scripts used for DGE and Functional Analysis are available in github repository: https://github.com/twisen/Orrantia-et-al-2022-RNASeq
- Any additional information required to reanalyze the data reported in this paper is available from the lead contact upon request.

EXPERIMENTAL MODEL AND SUBJECT DETAILS

Patients' characteristics and study design

Blood samples from 19 patients who suffered from MM and received autoHSCT were used in the study (Cohort 1. Age: median 59 and interquartile range 46-72; 10 males and 9 females). From them, samples from 10 patients were used for RNA-seq experiments, 3 samples were used for qPCR experiments and 6 samples were used for flow cytometry experiments. Samples were obtained at three different time points: T1 was collected the day before starting with the conditioning treatment; T2 was collected after leukocyte recovery (>1000 leukocytes/μL) and T3 was collected 30 days after cell infusion. MM patients' (cohort 1) clinical data can be found in Table 1. In addition, blood samples from a heterogeneous group of 6 patients that received an autoHSCT (Cohort 2. Age: median 58 and interquartile range 49-66; 4 males and 2 females) were used for flow cytometry experiments. Information about patients from cohort 2 is in Table 2. Moreover, buffy coats from anonymous healthy adult donors were used. Sample collection was carried out through the Basque Biobank for Research (http://www.biobancovasco.org), which complies with the quality management, traceability and biosecurity set out in the Spanish Law 14/2007 of Biomedical Research and in the Royal Decree 1716/2011. The study was approved by the Basque Ethics Committee for Clinical Research (BIO14/TP/003 and PI + CES + INC-BIOEF, 2017-03). All subjects provided written and signed informed consent in accordance with the Declaration of Helsinki.

METHOD DETAILS

Sample preparation

Peripheral blood mononuclear cells (PBMCs) were isolated from blood samples or buffy coats by Ficoll (GE Healthcare) density gradient centrifugation and cryopreserved in heat-inactivated Fetal Bovine Serum (FBS) (GE Healthcare Hyclone) containing 10% Dimethyl sulfoxide (DMSO) (Thermo Scientific Scientific).

NK cell isolation

Cryopreserved PBMCs were thawed at 37ºC in a water bath, washed with PBS (Lonza), filtered using 70μm cell strainers and counted. Next, PBMCs were stained with LIVE/DEAD Fixable Green Cell Stain Kit (Invitrogen) to exclude dead cells, following manufacturer's recommendations. Then, cells were washed with PBS containing 2.5% BSA (Sigma-Aldrich). Extracellular staining was carried out by incubating PBMCs for 30 min on ice in the dark with the following fluorochrome-conjugated monoclonal antibodies: PE anti-CD3 (UCHT1), PE anti-CD14 (MφP9), PE anti-CD19 (HIB19) and PE-Cy5 anti-CD56 (B159) from BD Bioscience and PEVio770 anti-NKp80 (4A4.D10) from Miltenyi Biotec. NK cells were identified as viable

CD3-/CD14-/CD19-/NKp80+/CD56$^{+/-}$ cells (Orrantia et al., 2020, 2021) and sorted using a BD FACSJazz cell sorter (Figure S4).

RNA extraction and sequencing

Total RNA was isolated from the sorted NK cells using RNeasy Plus Micro Kit (Qiagen) following manufacturer's recommendations. Quality and integrity of each RNA sample was checked using both a Bioanalyzer and a Nanodrop before proceeding to RNAseq protocol. 0.5 ng of total RNA were used to generate barcoded RNA-seq libraries using the NEBNext Single Cell/Low Input RNA Library Prep Kit for Illumina (New England Biolabs). Briefly, poly A + RNA was purified using poly-T oligo-attached magnetic beads followed by fragmentation and then first and second cDNA strand synthesis. Next, cDNA 3' ends were adenylated and the adapters were ligated and performed an uracile excision from the adaptor followed by PCR amplification. The size of the libraries was checked using the Agilent 2100 Bioanalyzer High Sensitivity DNA chip and their concentration was determined using the Qubit fluorometer (ThermoFisher Scientific). Libraries were sequenced on a HiSeq 2500/HiSeq4000 (Illumina) to generate 49/60 bases single reads. FastQ files for each sample were obtained using bcl2fastq 2.20 Software software (Illumina).

Reverse transcription (RT) reaction

cDNA was synthetized from 3 ng of total RNA using Super-Script IV VILO Master Mix with ezDNase enzyme (ThermoFisher Scientific) following manufacturer's recommendations. A DNA removal step is performed using ezDNase before the reverse transcription.

Real time qPCR

Real time qPCR was performed using Brilliant III Ultra-Fast SYBR Green qPCR Master Mix (Agilent Technologies) following manufacturer's recommendation on an Agilent AriaMX instrument (Agilent Technologies). In each reaction, 2 μL of (1:10) diluted cDNA of each sample was loaded in triplicates into Micro-Amp Fast 96-well reaction plates (Applied Biosystems). In addition, 18 μL of qPCR master mix was added, which included Brilliant III Ultra-Fast SYBR Green qPCR Master Mix (10 μL), housekeeping gene/probe gen primers (600nM of each primer were used), and nuclease free DEPC-treated water (Fisher Scientific). Negative controls (no cDNA) were included to verify the absence of contamination. Quantitative analysis was made based on the cycle threshold (Ct) value and calculated using AriaMX Real Time software v.A1.2 (Agilent Technologies). Ct mean values from triplicate reactions were calculated for further analysis. The sequences of the primers used are shown in Table S1. *PPIA* was used as housekeeping gene. Primers were designed with Primer3Plus software using FASTA sequences of each gene and synthetized by Invitrogen (Thermo Fisher).

Flow cytometry: Functional assay

For functional assay, PBMCs were thawed, counted, plated at 1×10^6 cells/well in 48-well plates in NK cell culture medium (RPMI 1640 medium with GlutaMAX, 10% heat-inactivated FBS, 1% penicillin-streptomycin, 1% non-essential amino acids and 1% Sodium-Pyruvate) and cultured overnight. Next, cells were stimulated with 50 ng/mL PMA and 2 μM Ionomycin for 6h. APC-Vio770 anti-CD107a (REA792, Miltenyi Biotec) was added at the start of the stimulation time in addition to GolgiStop (monensin) and GolgiPlug (brefeldin A) protein transport inhibitors (BD Biosciences) following manufacturer's recommendations. Next, PBMCs were washed with PBS and stained with LIVE/DEAD Fixable Aqua Dead Cell Stain Kit (Invitrogen) reagent to exclude dead cells, following manufacturer's recommendations. Afterward, cells were washed with PBS containing 2.5% BSA (Sigma-Aldrich) and extracellular staining was performed. For that, cells were incubated for 30 min on ice protected from light with the following fluorochrome-conjugated mAbs: BV510 anti-CD14 (MφP9), BV510 anti-CD19 (SJ25C1), BV510 anti-CD123 (9F5) and BV786 anti-CD56 (NCAM 16.2) from BD Biosciences; PE/Dazzle 594 anti-CD9 (HI9a) and PerCP-Cy5.5 anti-CD3 (SK7) from BioLegend and PE-Vio770 anti-NKp80 (4A4.D10) from Miltenyi Biotec. Cells were then washed again with PBS containing 2.5% BSA, and fixed and permeabilized using Cytofix/Cytoperm Fixation/Permeabilization solution from BD Biosciences following manufacturer's recommendations. Next, cells were incubated for 30 min on ice protected from light with the following fluorochrome conjugated mAbs: BV421 anti-IL-8 (G265-8), BV605 anti-IFNγ (B27), BV650 anti-IL-10 (JES3-9D7), FITC anti-MIP1β (D21-1351), R718 anti-granzyme B (GB11) from BD Bioscience; BV711 anti-perforin (dG9) and APC anti-TNF (Mab11) from BioLegend. Finally, cells were washed with 1x Perm/Wash Buffer (BD Biosciences) and resuspended in

PBS. Samples were then acquired in a LSRFortessa X-20 flow cytometer (BD Biosciences). Flow cytometry panel used for the functional assay is shown in Table S2.

For the functional assay with the 721.221 target cell line we followed a protocol previously published by us (Orrantia et al., 2021). Briefly, after thawing and counting the PBMCs, cells in NK cell culture medium were plated at 0.5 x 10^6 cells/well in 96 well round (U) bottom plates. PBMCs were then primed with 10 ng/mL of recombinant human (rh) interleukin (IL)-15 (Miltenyi Biotec) and cultured overnight. Then, 721.221 target cells were added at Effector:Target (E:T) 1:1 ratio (0.5x10^6 PBMCs and 0.5x10^6 721.221 target cells) and cultured for 8 additional hours. APC-Vio770 anti-CD107a was added at the start of the co-culture period and GolgiStop and GolgiPlug were added 1 h later. Next, extracellular and intracellular staining was performed as above described for PMA and ionomycin stimulation. However, in this set of experiments a different panel of antibodies were used (see Tables S2 and S3).

QUANTIFICATION AND STATISTICAL ANALYSIS

RNA-seq data analysis

Sequencing reads were aligned to the human reference transcriptome (GRCh38 v91) and quantified with RSem v1.3.1 (Li and Dewey, 2011). Raw counts were normalized with TPM (Transcripts per Million) and TMM (Trimmed Mean of M-values) methods, transformed into log2 expression (log2(rawCount+1)) and compared to calculate fold-change and corrected p Value. Only those genes expressed with at least 1 count in 8 samples equal were taken into account. As we had an expected intra-group variability, we considered for functional analysis genes with |Log2FC| > 0.58 and unadjusted p Value <0.05, although we also calculate the Benjamini and Hochberg correction for all genes. The source code for the analysis is available in the github repository: https://github.com/twisen/Orrantia-et-al-2022-RNASeq.

Heatmaps were generated with Morpheus online tool from Broad Institute (https://software.broadinstitute.org/morpheus). For functional analysis, we used clusterProfiler (version 3.18.1), ReactomePA (version 1.34.0) and pathview R (version 1.30.1) packages (Luo and Brouwer, 2013; Yu et al., 2012; Yu and He, 2016).

Flow cytometry data analysis

Flow cytometry data were analyzed using FlowJo v10.8.1. software. GraphPad Prism v.9.3.1 was used for graphical representation and statistical analysis. Non-parametric Wilcoxon matched-pairs signed rank test were used to determine significant differences. Data were represented as bar plots showing the median and interquartile range.